A dangerous trade-off? Phase instability and porosity in Ti-Rich Al$_2$O$_3$-Ti composites

Justyna Zygmuntowicz[1]*, Marcin Wachowski[2], Paulina Piotrkiewicz[1], Waldemar Kaszuwara[1], Bartosz Michalski[1], Paweł Falkowski[3], Radosław Żurowski[3]

[1] Faculty of Materials Science and Engineering, Warsaw University of Technology, ul. Woloska 141, 02-507 Warsaw, Poland
[2] Faculty of Mechanical Engineering, Military University of Technology, ul. gen. S. Kaliskiego 2, 00-908 Warsaw, Poland
[3] Faculty of Chemistry, Warsaw University of Technology, ul. Nowakowskiego 3, 00-664 Warsaw, Poland
* Corresponding author's e-mail: justyna.zygmuntowicz@pw.edu.pl

ABSTRACT

This study examined the effect of titanium content on the processing and microstructural evolution of the Al$_2$O$_3$-Ti composites fabricated by slip casting. Two compositions with 1 vol.% and 10 vol.% Ti were investigated. Rheological tests revealed that a low Ti content increased slurry viscosity, but promoted more uniform packing and densification. After sintering at 1400 °C, the 1 vol.% Ti composites achieved high relative density (>93%), negligible open porosity, and formation of a stable Ti$_{0.25}$Al$_{1.75}$O$_3$ phase. In contrast, the 10 vol.% Ti composites showed poor densification (~77%), high porosity, and the presence of unstable Al$_2$TiO$_5$ and residual TiO$_2$. These results demonstrate that 1 vol.% Ti is optimal for producing dense, defect-free Al$_2$O$_3$-Ti composites, while excessive Ti content leads to phase instability and microstructural degradation. The findings highlight slip casting as a viable method for designing alumina-based composites with tailored phase composition, offering the potential for structural, thermal, and biomedical applications where both durability and reliability are required.

Keywords: slip casting, composites, Al$_2$O$_3$-Ti, rheological properties.

INTRODUCTION

Ceramic–metal composites are multifunctional materials that combine the hardness, chemical stability, and thermal resistance of ceramics with the toughness, electrical conductivity, and ductility of metals [1–4]. This hybrid character allows them to overcome the brittleness of ceramics and the limited high-temperature strength of metals [5–6], enabling their use in demanding applications, such as cutting tools, wear-resistant parts, thermal barrier coatings, electrical contacts, and biomedical implants [7–9].

Within this group, Al$_2$O$_3$-Ti composites are of particular interest, because of the complementary properties of the two phases [10–13]. Alumina provides high hardness, wear resistance, and chemical inertness [14–16], while titanium offers high specific strength, corrosion resistance, and improved toughness due to strong interfacial bonding with the ceramic matrix [17–21]. Furthermore, Ti additions can enhance thermal shock resistance and contribute to crack deflection and bridging mechanisms, thereby improving fracture toughness [21–22]. These combined features make the Al$_2$O$_3$-Ti composites suitable for structural, thermal, and biomedical applications, including armor materials, aerospace protection systems, spark plug insulators, and prosthetic components [23–26]. Various fabrication techniques are employed to produce Al$_2$O$_3$-Ti composites, each providing specific benefits depending on the targeted microstructure and properties [27–31].

Slip casting is a versatile and cost-effective forming method that enables fabrication of dense, complex-shaped ceramic components [32–34].

Its application to ceramic–metal systems provides advantages, such as homogeneous phase distribution, scalability, and near-net-shape production at relatively low cost [35–38]. However, challenges remain, including particle agglomeration, sedimentation of metallic particles, and interfacial reactions during sintering, which require careful control of solid loading, particle size distribution, and suspension rheology [38].

This work investigated the preparation and microstructural evolution of Al_2O_3-Ti composites fabricated via slip casting with varying titanium content. The study aimed to understand how the volume fraction of the metallic phase influences the homogeneity of phase distribution, the interfacial interactions, and the resulting composite microstructure. Scanning electron microscopy (SEM) combined with energy-dispersive X-ray spectroscopy (EDS) is employed to characterize the chemical composition and dispersion of the metallic phase. The findings contribute to the development of tailored Al_2O_3-Ti composites for structural, thermal, and biomedical applications, where performance depends critically on microstructural control and phase integrity.

The present work bridged a critical gap in the development of ceramic–metal composites by systematically examining how the volume fraction of titanium affects the processing, phase evolution, and microstructural quality of Al_2O_3-Ti systems fabricated via slip casting. While numerous studies have investigated the Al_2O_3-Ti composites produced by hot pressing, spark plasma sintering, or powder metallurgy, only limited attention has been given to slip casting, despite its potential as a cost-effective and scalable forming technique. Previous reports have focused mainly on mechanical properties, without establishing clear correlations between slurry rheology, densification, phase composition, and microstructural evolution [37].

This manuscript introduces several novel aspects. First, it demonstrates how the rheological behavior of the casting slip directly influences particle packing, porosity, and shrinkage during sintering. By comparing the composites with 1 vol.% and 10 vol.% Ti, the study showed that higher Ti content reduces viscosity but promotes sedimentation, leading to poor densification and anisotropic shrinkage. Second, the work provides new insight into Ti-dependent phase transformations: at low Ti content, Ti is fully consumed to form $Ti_{0.25}Al_{1.75}O_3$, while higher Ti loadings favor the formation of Al_2TiO_5 and residual TiO_2, phases associated with

instability and microstructural degradation. The key premise of this research is that optimizing metallic phase content is essential not only for mechanical performance but also for processing reliability. By establishing a direct link between slurry preparation, microstructure, and phase stability, this study contributes new knowledge for designing the Al_2O_3-Ti composites with improved structural integrity and application potential.

MATERIALS AND METHODOLOGY

Two commercially available powders were used as the starting materials for the fabrication of Al_2O_3-Ti composite samples via the slip casting method. The ceramic matrix was based on high-purity alumina (Al_2O_3, TM-DAR, Taimei Chemicals Co., Ltd.), characterized by an ultra-fine average particle size in the range of 0.05–0.2 μm, a density of 3.89 g/cm³, and a purity of ≥99.99%. This powder is well-known for its excellent dispersion behavior and high reactivity, making it particularly suitable for colloidal processing techniques, such as slip casting. The metallic phase was introduced in the form of titanium powder (Ti, GoodFellow Cambridge Limited, UK), with a nominal average particle size of 75 μm, a bulk density of 4.51 g/cm³, and a purity of 99.50%. The substantial size difference between the alumina and titanium particles was deliberately selected to study the influence of phase distribution and packing behavior on the microstructural and physical properties of the resulting composites.

The Al_2O_3-Ti composite samples were prepared using the aqueous slip casting method. On the basis of the required volume fraction of the metallic phase, two series of compositions were formulated: Series I containing 1 vol.% Ti and Series II containing 10 vol.% Ti. The total solid content of the suspensions was kept constant at 50 vol.% for all samples. The slurries were prepared by first dispersing the appropriate amount of Al_2O_3 powder (TM-DAR, Taimei Chemicals, average particle size 0.05–0.2 μm, purity ≥99.99%) and Ti powder (GoodFellow Cambridge Limited, average particle size 75 μm, purity 99.50%) in deionized water. To ensure stable dispersion and prevent agglomeration, a suitable amount of a commercial dispersant, such as citric acid (CA) and diammonium citrate (DAC), was added to the suspension. The mixed suspensions were homogenized using a planetary ball mill for 1 hour

at room temperature to ensure uniform dispersion of both ceramic and metallic phases. Following milling, the slurries were de-aired under vacuum to remove entrapped air bubbles (for this purpose, a THINKY ARE-250 high-speed homogenizer (Tokyo, Japan) was used) and poured into cylindrical plaster molds. Capillary action from the mold surface facilitated water removal, leading to the gradual deposition of solid particles and the formation of green bodies. After drying under ambient conditions for 48 hours, the samples were demolded and subsequently subjected to controlled drying at 60 °C to eliminate residual moisture. The dried green bodies were then sintered in an Argon atmosphere. The sintering of the Al_2O_3-Ti composite samples was performed using a high-temperature tube furnace (model RFTC 80230/16, Nabertherm GmbH, Lilienthal, Germany), equipped with silicon carbide heating elements arranged in parallel alignment along the working chamber. This configuration provided excellent temperature uniformity throughout the furnace volume. The thermal treatment was conducted in a multi-step heating regime. Initially, the temperature was raised from ambient (23 °C) to 120 °C at a rate of 5 °C/min to remove residual moisture. This was followed by a slower ramp to 750 °C at 1 °C/min to allow for controlled burnout of organic additives. Subsequently, the temperature was increased to the final sintering temperature of 1400 °C at a rate of 2 °C/min. The samples were held isothermally at 1400 °C for 2 hours to ensure sufficient densification. The cooling phase was carried out at a controlled rate of 5 °C/min to minimize thermal stresses and prevent cracking. The sintering temperature of 1400 °C was selected based on preliminary trials and supported by literature, which shows this temperature ensures sufficient densification of Al_2O_3-Ti composites without excessive grain growth.

The primary objective of this study was to investigate the influence of the metal phase content in the casting slip on the successive stages of composite fabrication and the resulting microstructural characteristics of the sintered materials. To achieve this, a comprehensive experimental approach was designed, encompassing the entire processing route – from slip preparation to final microstructural analysis. Different compositions of ceramic-metal slurries were prepared by systematically varying the volume fraction of the metallic phase (Ti) (1 vol.% and 10 vol.%), while keeping all other parameters constant. This

allowed for the isolation and analysis of the effect of metal phase on key aspects of the fabrication process, including slip stability, rheological behavior, casting quality, sintering response, and microstructural evolution. A series of complementary characterization techniques was employed, including rheological measurements to assess slurry flow behavior and stability, physical property measurements (density, porosity, water absorption) using the Archimedes method, X-ray diffraction (XRD) to monitor phase composition before and after sintering, Scanning electron microscopy (SEM) combined with energy-dispersive X-ray spectroscopy (EDS) to analyze microstructure and elemental distribution, and image analysis to quantify grain growth behavior and particle distribution. This multi-technique approach enabled a detailed understanding of how variations in metal content influence the processing and final properties of the Al_2O_3-Ti composites.

Rheological measurements were carried out to evaluate the flow behavior and structural stability of the prepared ceramic-metal casting slips. The tests were performed using a Kinexus Pro rotational rheometer (Malvern Instruments, UK) equipped with a plate–plate measuring system, which is well-suited for characterizing suspensions and slurries. The measurements were conducted at room temperature under controlled conditions to ensure repeatability and comparability of results. A gap height of 0.5 mm was maintained between the plates during all tests. To prevent edge drying effects and ensure consistent measurement conditions, poly (dimethylsiloxane) (PDMS) oil (Sigma-Aldrich) was carefully applied around the perimeter of the sample. This inert, non-miscible fluid formed a protective barrier without interfering with the rheological properties of the suspension. The dynamic viscosity of the casting slips was measured as a function of shear rate, allowing the determination of flow curves and assessment of shear-thinning or thickening behavior, which is critical for evaluating the processability of the slips during shaping. The obtained rheological data supported the optimization of slip formulations for improved casting performance and structural integrity of the green bodies.

The selected physical properties of the sintered composite samples, including relative density, water absorption, and open porosity, were determined using the Archimedes method in accordance with standard procedures for ceramic materials. The measurements were carried out by

immersing the sintered samples in distilled water to determine their buoyant mass and saturated weight. Initially, the dry weight of each sample was recorded. The samples were then boiled in water to remove trapped air from open pores and subsequently soaked under vacuum to ensure full saturation. The saturated weight in air and the suspended weight in water were then measured. These values were used to calculate the open porosity and water absorption. At the same time, the relative density was determined by comparing the bulk density of the sample to the theoretical density of the composite, taking into account the proportions of Al_2O_3 and Ti. This method provides reliable insight into the compactness and integrity of the sintered structure and allows for evaluation of the efficiency of the densification process.

The microstructure of the sintered composite samples was examined using scanning electron microscopy (SEM) to evaluate the morphology, distribution of phases, and overall microstructural integrity. Observations were carried out using a JEOL JSM-6610 scanning electron microscope, operated at an accelerating voltage of 15 kV, which provided high-resolution imaging suitable for detailed surface and cross-sectional analysis. The SEM observations focused on identifying the distribution and morphology of the metallic phase (Ti) within the ceramic matrix (Al_2O_3), grain boundaries, porosity, and potential interfacial reactions or defects formed during the sintering process. In parallel, the chemical composition of the selected microstructural features was investigated using Energy Dispersive X-ray Spectroscopy (EDS), integrated with the SEM system. EDS analysis enabled the identification and semi-quantitative assessment of elemental constituents present in different regions of the composites. This was particularly important for confirming the presence and dispersion of the Ti phase, detecting any unwanted secondary phases, and evaluating elemental diffusion at the ceramic–metal interfaces. Together, SEM and EDS analyses provided complementary information about the microstructural development and phase distribution in the sintered composites.

The phase composition of the composite materials was examined using X-ray diffraction to identify the crystalline phases present before and after the sintering process. The analysis was performed with a Rigaku Miniflex II X-ray diffractometer equipped with a Cu Kα radiation source (λ = 1.5406 Å). The XRD measurements were conducted over a 2θ angular range of 20° to 100°, using a step size of 0.03° and a counting time of 1 second per step. These parameters were selected to ensure high-resolution detection of diffraction peaks and to enable accurate phase identification. The resulting diffractograms were analyzed using the MDI Jade 8.9 software, integrated with the PDF-5+ 2024 crystallographic database. This combination enabled precise identification of both major and minor phases within the samples. Each sample was analyzed under two conditions: in the as-prepared (raw) state and after the sintering process. This dual-stage analysis was performed to detect any phase transformations, reactions between the ceramic and metallic components, or formation of secondary phases induced by thermal treatment. Comparison of the XRD patterns before and after sintering provided insights into the thermal stability of the constituent phases and the integrity of the composite structure under processing conditions.

A detailed image analysis was conducted to evaluate the influence of the metallic phase content on the microstructural evolution of the sintered composites. This analysis aimed to quantify the growth behavior of Al_2O_3 grains in relation to varying contents of the metal phase (Ti) introduced into the casting slips. The examination was carried out on the fracture of sintered samples using high-resolution scanning electron microscopy. The acquired micrographs were subjected to quantitative image analysis using the Micrometer software package [39–42], which is specifically designed for microstructural characterization of polycrystalline materials. Within this analysis, key parameters such as average grain size and grain size distribution were extracted. A thresholding technique was employed to differentiate between the ceramic matrix (Al_2O_3) and the metallic inclusions (Ti), ensuring accurate grain segmentation. Subsequent measurements were performed on multiple fields of view per sample to achieve statistical relevance.

RESULTS

Figure 1a) shows nanometric alumina particles (TM-DAR, Taimei Chemicals) characterized by a high degree of agglomeration. The individual particles exhibit a near-spherical morphology with sizes typically below 200 nm. The observed agglomerates are formed due to strong interparticle interactions common in ultrafine powders,

which can influence the dispersion stability and rheological properties of the casting slurry. The scale bar corresponds to 0.5 µm. At the same time, Figure 1b) presents Ti powder (Goodfellow) with an irregular, angular morphology and a much coarser size distribution compared to the alumina powder. The Ti particles appear as fractured flakes and granules, ranging in size from a few micrometers up to approximately 100 µm. This morphology may affect the packing behavior and sedimentation during slip casting. The scale bar corresponds to 100 µm.

The first stage of laboratory work involved characterizing the obtained suspensions in terms of their basic rheological properties. The determined viscosity curves (Figure 2a) and flow curves (Figure 2 b) demonstrate that both samples exhibit shear-thinning properties and slight thixotropic properties. The presented profiles of both viscosity and flow curves are typical for ceramic suspensions (and suspensions of ceramic powders doped with metal particles), and the obtained results correlate well with literature data [43-47]. When analyzing the data presented in Figure 2a and Table 1, it is worth noting the differences in the viscosity of both suspensions, which are particularly visible at low shear rates. The sample doped with 1 vol.% Ti (and therefore containing significantly more nano-Al_2O_3) is characterized by a significantly higher viscosity compared to the suspension modified with as much as 10 vol.% Ti.

Quantitatively, dynamic viscosity measurements at various shear rates (Table 1) reveal distinct differences between the two compositions. At a low shear rate of 0.1 s^{-1}, Series I (1 vol.% Ti) exhibits a significantly higher viscosity (19.6 Pa·s) than Series II (10 vol.% Ti), which has a viscosity of 13.0 Pa·s. This trend is maintained across all tested shear rates, though the difference narrows as shear increases, with viscosities converging at 100 s^{-1} (0.39 Pa·s for Series I vs. 0.33 Pa·s for Series II). The higher viscosity of Series I is likely due to its greater content of nano-sized Al_2O_3 particles, which possess a higher specific surface area and stronger interparticle interactions compared to the more metallic-rich Series II. These interactions promote greater resistance to flow, particularly at lower shear rates, where structure breakdown is minimal. The observed differences between Series I and Series II were larger than the measurement uncertainty, and therefore statistically significant.

The observed rheological behavior confirms that both suspensions are suitable for slip casting. The shear-thinning nature ensures ease of processing under applied shear, while thixotropy supports shape retention post-casting.

The physical properties of the Al_2O_3-Ti composite samples prepared via slip casting are summarized in Table 2. Two series of samples were analyzed: Series I with 1 vol.% Ti and Series II with 10 vol.% Ti. A comparison of the results reveals a significant influence of titanium content on the densification behavior and microstructural development of the composites.

Theoretical densities for the two series increased marginally with higher Ti content, from 3.99 g/cm³ for Series I to 4.04 g/cm³ for Series II, which is consistent with the higher density of titanium compared to alumina. However, the relative density exhibited a marked decrease with increasing Ti content. Series I achieved a relative density of 93.65 ± 0.29%, indicating successful sintering and good particle packing. In contrast, Series II displayed a substantially lower relative density of 76.69 ± 0.73%, suggesting limited densification and the presence of significant
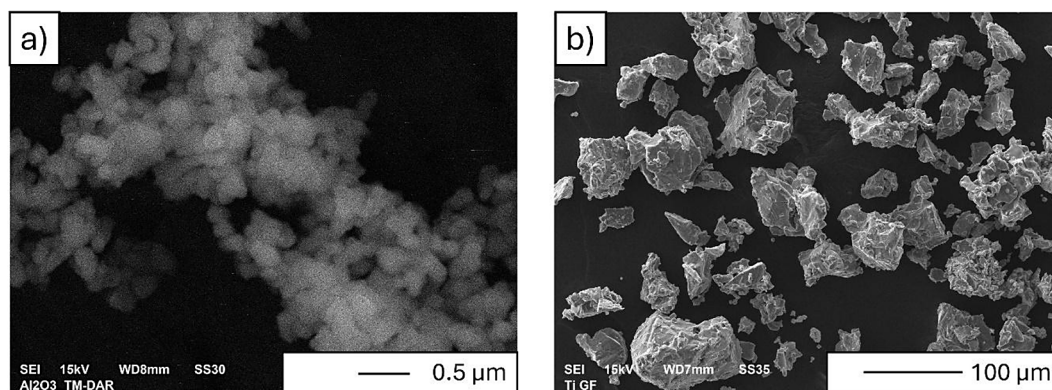
Figure 1. Scanning electron microscopy images of the starting powders used for the fabrication of Al_2O_3-Ti composites via slip casting. (a) TM-DAR alumina particles; (b) titanium powder

a)

b)
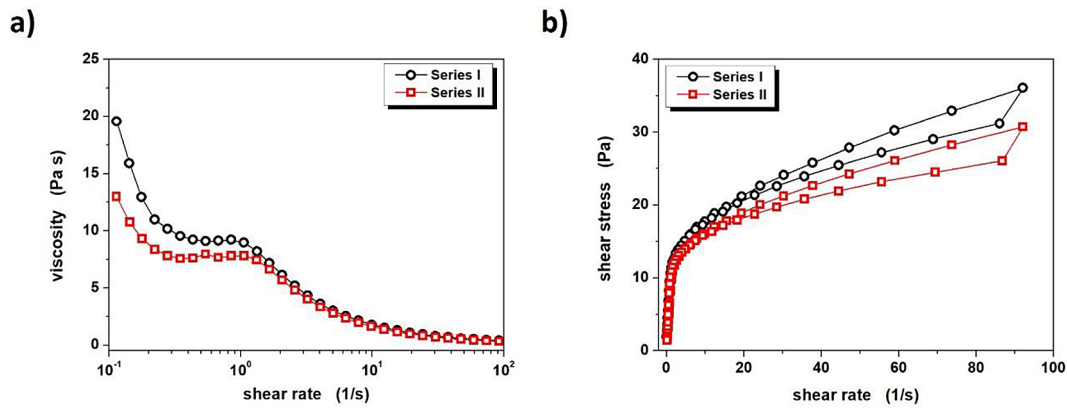
Figure 2. Flow curves (a) and viscosity curves (b) of the prepared ceramic suspensions:
Series I – 1% vol. of Ti; Series II – 10% vol. of Ti

porosity. Open porosity and water absorption measurements further support this observation. Series I exhibited negligible open porosity (0.27 ± 0.12%) and minimal water absorption (0.07 ± 0.03%), indicative of a dense, nearly pore-free microstructure. On the other hand, Series II showed markedly higher values of open porosity (8.21 ± 0.57%) and water absorption (2.65 ± 0.17%), confirming the presence of interconnected pore networks likely formed due to inefficient packing and hindered sintering at higher titanium content.

Shrinkage measurements provided additional insights into the sintering response. Series I exhibited significant linear shrinkage along both the sample diameter (13.16 ± 0.35%) and height (10.08 ± 1.02%), as well as substantial volumetric shrinkage (31.28 ± 1.23%). These values are consistent with the expected behavior of a well-densified ceramic body undergoing uniform sintering. Conversely, The Series II samples experienced minimal linear shrinkage (3.09 ± 0.93% in diameter and 1.97 ± 1.23% in height) and low volumetric shrinkage (8.49 ± 1.03%), reflecting limited particle rearrangement and consolidation during sintering. The discrepancy between shrinkage in diameter and height also suggests anisotropic behavior, potentially due to gravitational settling or agglomeration of heavier Ti particles during slip casting.

The inferior densification and increased porosity observed in Series II may be attributed to several factors. A high concentration of Ti particles can hinder the homogeneity of the slurry and disrupt the packing efficiency during casting. Moreover, the mismatch in thermal expansion coefficients between Ti and Al_2O_3 may induce localized stresses during heating, leading to microcrack formation or particle pull-out. Agglomeration of the metallic phase and weak interfacial bonding may act as diffusion barriers, limiting sintering kinetics and promoting porosity.

In contrast, the low Ti content in Series I appears to be within the optimal range for effective dispersion and integration of the metallic phase within the alumina matrix, promoting enhanced sintering behavior and superior microstructural quality. These findings underscore the critical role of Ti volume fraction in determining the densification efficiency and final properties of the Al_2O_3-Ti composites produced by slip casting.

The results indicate a strong correlation between slurry rheology and the final microstructural quality of the sintered composites. The higher viscosity of the Series I suspension likely promoted more uniform particle packing and minimized sedimentation during slip casting, contributing to improved densification and microstructural integrity. In contrast, the lower-viscosity Series II suspension, despite being easier to process, may

Table 1. Dynamic viscosity values of the prepared ceramic suspensions for shear rates of 0.1, 1, 10, and 100 s^{-1}

Series	Viscosity at shear rate 0.1 s^{-1}	Viscosity at shear rate 1 s^{-1}	Viscosity at shear rate 10 s^{-1}	Viscosity at shear rate 100 s^{-1}
	Pa·s			
Series I	19.6 ± 0.03	8.96 ± 0.07	1.79 ± 0.05	0.39 ± 0.03
Series II	13.0 ± 0.05	7.81 ± 0.04	1.64 ± 0.02	0.33 ± 0.02

Table 2. Theoretical and measured physical properties of the Al_2O_3-Ti composite samples formed by slip casting. The data include theoretical density, relative density, open porosity, water absorption, and linear and volumetric shrinkage for samples with 1 vol.% (Series I) and 10 vol.% (Series II) of Ti

Series	Theoretical density	Relative density	Open porosity	Water absorption	Linear shrinkage measured along the sample diameter	Linear shrinkage measured along the sample height	Volumetric shrinkage
	g/cm³	%	%	%	%	%	%
Series I (1 vol.% of Ti)	3.99	93.65 ± 0.29	0.27 ± 0.12	0.07 ± 0.03	13.164 ± 0.35	10.08 ± 1.02	31.28 ± 1.23
Series II (10 vol.% of Ti)	4.04	76.69 ± 0.73	8.21 ± 0.57	2.65 ± 0.17	3.09 ± 0.93	1.97 ± 1.23	8.49 ± 1.03

have experienced increased phase segregation and settling of the heavier Ti particles, ultimately resulting in poor green body homogeneity and compromised sintering performance.

These findings highlight the importance of tailoring slurry rheology to control green body structure, which in turn influences the densification and final properties of composite ceramics. Optimizing the volume fraction of the metallic phase and the solid loading of ceramic particles is essential for achieving a balance between processability and final material quality.

Although the present study did not include direct measurements of hardness, strength, or fracture toughness, the microstructural findings allow for a preliminary assessment of the expected mechanical behavior. The dense and homogeneous microstructure of the 1 vol.% Ti composites, with relative density above 93% and negligible porosity, suggests that these materials would exhibit favorable mechanical performance, particularly in terms of strength and resistance to crack propagation. In contrast, the 10 vol.% Ti composites, characterized by high open porosity (~8%), agglomeration of metallic particles, and the presence of Al_2TiO_5 are expected to display significantly reduced strength and toughness. The formation of Al_2TiO_5, which is prone to anisotropic thermal expansion and microcracking, further compromises structural integrity. For these reasons, reliable mechanical testing of Series II was not feasible within the current work, as high porosity leads to large variability and poor reproducibility of results. Nevertheless, the observed correlations between rheological behavior, densification, and phase composition provide a strong indication that optimizing the Ti content is essential for achieving composites with both high density and reliable mechanical performance. Comprehensive mechanical testing will be the focus of authors' future investigations.

SEM observations revealed that the composite containing 1 vol.% Ti (Figure 3a) shows a relatively dense microstructure with well-sintered alumina grains and isolated residual pores. The Ti particles are sparsely distributed and embedded within the alumina matrix, visible as localized regions of contrast. The high-magnification image reveals that titanium is primarily surrounded by a continuous Al_2O_3 phase, and appears partially sintered and oxidized, potentially forming a thin interfacial layer, possibly TiO_2. The interface between Ti and the ceramic matrix is relatively clean, with minimal porosity or cracking, indicating satisfactory wetting and bonding at this low content.

In contrast, the composite with 10 vol.% Ti (Figure 3 b) displays a significantly more porous and heterogeneous microstructure. The top-view SEM image reveals a larger number of dark regions corresponding to increased porosity and more frequent Ti agglomerations. At high magnification, the Ti regions exhibit poor interfacial bonding with the matrix, as evidenced by voids, irregular pore shapes, and microcracking around the particles. The titanium particles appear partially sintered, occasionally oxidized, with clear evidence of pull-out and shrinkage-induced porosity. The grain boundaries of alumina in the vicinity of Ti particles are more irregular compared to the 1 vol.% sample, likely due to localized stress concentrations and sintering behavior.

Overall, increasing the Ti content from 1 vol.% to 10 vol.% significantly deteriorates microstructural homogeneity and densification quality. The higher metallic phase fraction leads to agglomeration, poor dispersion, and enhanced porosity formation during sintering, which may negatively impact the mechanical performance of the composite. This highlights the importance of optimizing the Ti content and particle dispersion in order to achieve a uniform, well-bonded ceramic-metal microstructure. It should be emphasized
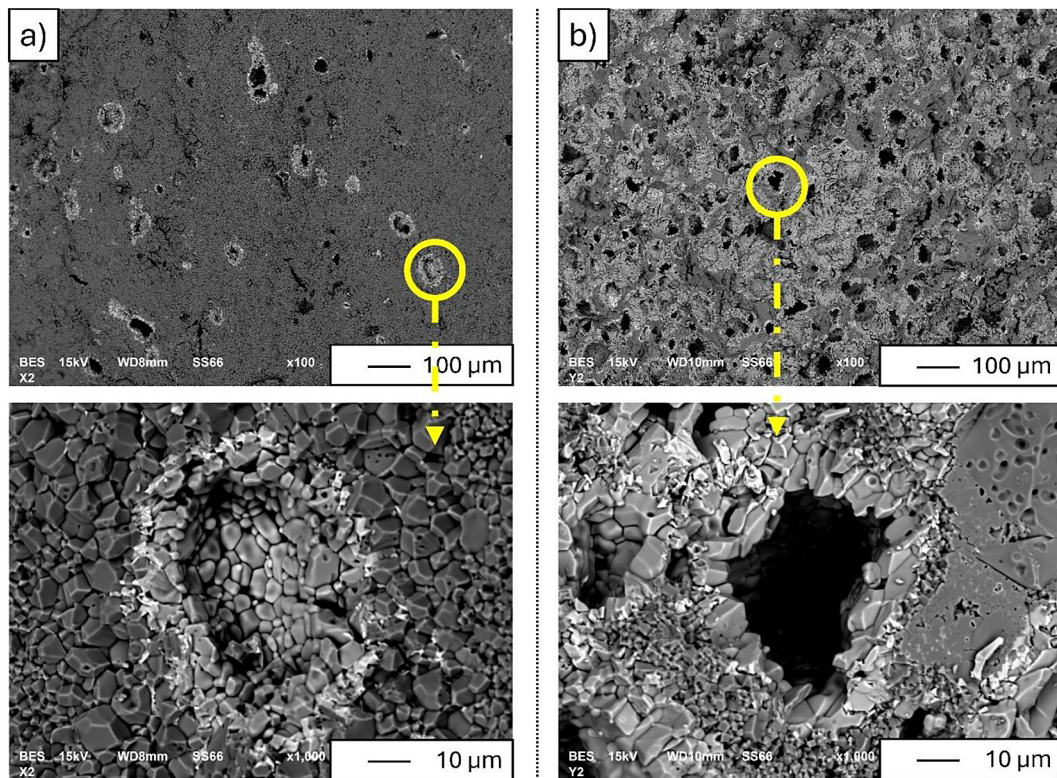
Figure 3. SEM micrographs of the sintered Al_2O_3-Ti composites fabricated by slip casting, observed at low and high magnifications: (a) the composite with 1 vol.% Ti, (b) the composite with 10 vol.% Ti

that while the distribution of Ti particles in Series II appears more uniform due to higher volume fraction, this apparent homogeneity is offset by high porosity and poor bonding, leading to inferior structural integrity.

Figures 4a and b present the microstructures of the composite samples from Series I and Series II, containing 1 vol.% and 10 vol.% of the metallic phase, respectively. Both figures are accompanied by point-wise energy-dispersive X-ray spectroscopy (EDS) analyses (summarized in Table 3), which reveal the elemental composition of selected areas and provide insight into the distribution and incorporation of the metallic phase within the alumina matrix.

In Series I (Figure 4a), the microstructure is characterized by a predominantly ceramic (Al_2O_3) matrix with minimal visible metallic phase content. EDS point analyses confirm this observation: Area 1 consists exclusively of aluminum and oxygen (51.23 wt% Al, 48.77 wt% O), indicative of a pure alumina matrix. Areas 2 and 3, however, show the presence of titanium (19.78 wt% and 25.06 wt%, respectively), suggesting localized inclusion of the metallic phase in these regions. The relatively high oxygen content also points toward possible oxide formation or intermetallic

inclusions in those zones at the metal-ceramic interface or during processing.

In contrast, Series II (Figure 4b) exhibits a much higher density of metallic inclusions, in accordance with its 10 vol.% metallic phase content. The EDS results confirm these observations: Area 1 corresponds to a pure alumina matrix (53.42 wt% Al, 46.58 wt% O), comparable to Area 1 in Series I, while Areas 2 and 3 show the presence of titanium at slightly higher concentrations (23.21 wt% and 24.75 wt%, respectively), indicating more frequent and evenly distributed metallic regions.

The homogeneity of metallic phase distribution in Series II appears significantly improved compared to Series I. The more uniform distribution observed in Series II is likely due to the higher overall metallic content, which increases the probability of forming a continuous or semi-continuous metallic network within the matrix.

The EDS results indicate a clear trend: the incorporation of a higher volume fraction of the metallic phase not only increases the number of Ti-rich regions but also leads to more consistent and comparable chemical profiles across different analyzed areas. In Series I, the variation in Ti content between Area 2 and Area 3 (19.78 vs. 25.06
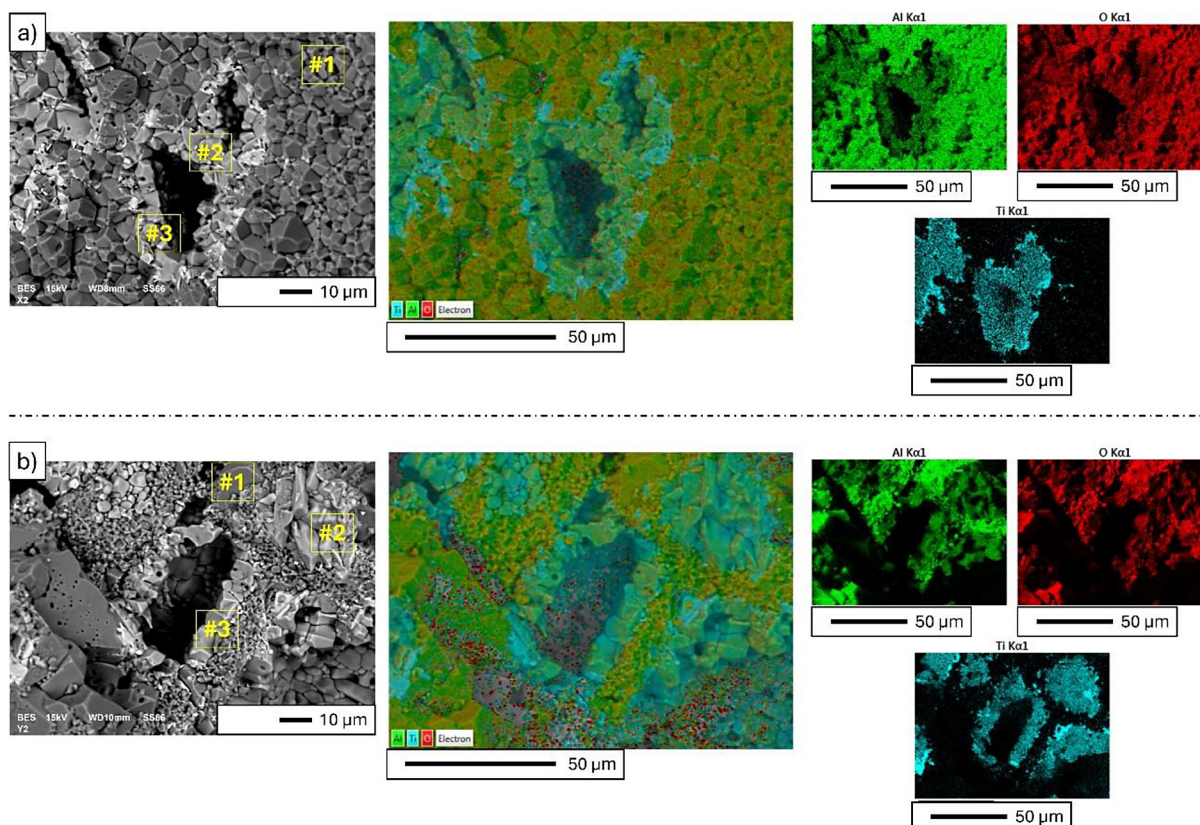
Figure 4. SEM micrographs of the Al_2O_3-Ti composites with varying metallic phase content: (a) Series I containing 1 vol.% of the metallic phase and (b) Series II containing 10 vol.% of the metallic phase. The marked areas indicate locations of EDS point analyses. A noticeable increase in the number and distribution uniformity of the metallic inclusions is observed in Series II compared to Series I

wt%) may reflect the inhomogeneities in metallic particle dispersion. Meanwhile, Series II shows a narrower range (23.21–24.75 wt% Ti), indicating a more uniform distribution.

The lower oxygen content in Areas 2 and 3 of Series II (compared to Series I) suggests a higher proportion of metallic titanium relative to the ceramic matrix or reduced oxidation of the metallic phase. The reduced oxygen content in Series II may influence interfacial bonding characteristics and ultimately affect the mechanical behavior of the composites.

In the next step, a phase analysis of the composites was performed before and after the sintering process. Figure 5 presents the X-ray diffraction patterns of the Al_2O_3-Ti composites recorded before and after sintering for both compositions: (a) Series I (1 vol.% Ti) and (b) Series II (10 vol.% Ti). The diffractograms provide direct insight into the phase composition of the green bodies and the phase transformations induced during high-temperature treatment. Before sintering, both series showed diffraction peaks corresponding to the starting materials, namely α-Al_2O_3 (JCPDS

46-1212) and metallic Ti (JCPDS 44-1294). The absence of additional diffraction peaks indicates that no significant reactions occurred during slurry preparation or drying. The relative peak intensities confirm that alumina constitutes the dominant crystalline phase in both systems.

In contrast, the weaker reflections from titanium are consistent with its relatively low volume fraction in the composites. After sintering at 1400°C, substantial differences in phase evolution were observed between the two series. In Series I (1 vol.% Ti), the titanium reflections disappeared completely, and new peaks associated with a ternary phase, $Ti_{0.25}Al_{1.75}O_3$, were detected. The emergence of this phase indicates that, under the applied sintering conditions, the limited amount of Ti reacted extensively with alumina, resulting in the formation of a stable Al-Ti-O compound. The complete consumption of metallic Ti indicates that at this low concentration, the diffusion and oxidation of titanium were sufficient to drive full reaction with the ceramic matrix.

In contrast, Series II (10 vol.% Ti) exhibited a markedly different behavior. After sintering,

Table 3. Chemical composition of selected areas (marked in Figures 4a and 4 b) determined by energy-dispersive X-ray spectroscopy (EDS). Results are presented as weight percent (wt%) and atomic percent (at%) for aluminum (Al), oxygen (O), and titanium (Ti). The data illustrate the differences in metallic phase presence and distribution between Series I (1 vol.%) and Series II (10 vol.%)

The measurement area is shown in Figure 4	Chemical composition					
	Al		O		Ti	
	Weight %	Atomic %	Weight %	Atomic %	Weight %	Atomic %
Area 1 (Figure 4a)	51.23 ± 0.16	61.62 ± 0.12	48.77 ± 0.16	61.62 ± 0.09	-	-
Area 2 (Figure 4a)	26.54 ± 0.14	20.70 ± 0.08	53.68 ± 0.20	70.61 ± 0.11	19.78 ± 0.16	8.69 ± 0.09
Area 3 (Figure 4a)	28.02 ± 0.17	23.11 ± 0.11	46.92 ± 0.25	65.25 ± 0.06	25.06 ± 0.19	11.64 ± 0.12
Area 1 (Figure 4b)	53.42 ± 0.17	40.48 ± 0.08	46.58 ± 0.17	59.52 ± 0.02	-	-
Area 2 (Figure 4b)	28.79 ± 0.11	23.44 ± 0.05	48.00 ± 0.16	65.92 ± 0.14	23.21 ± 0.13	10.65 ± 0.05
Area 3 (Figure 4b)	28.47 ± 0.12	23.47 ± 0.15	46.78 ± 0.18	65.04 ± 0.12	24.75 ± 0.14	11.49 ± 0.09
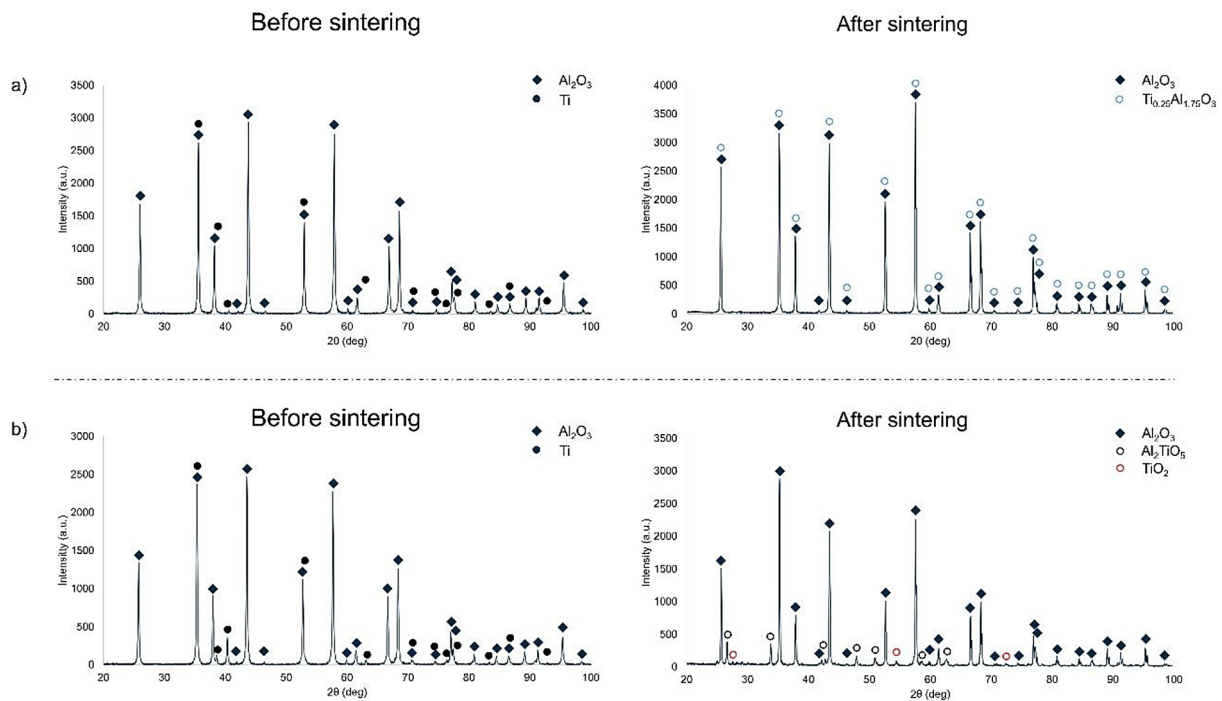
Figure 5. X-ray diffraction patterns of the Al_2O_3-Ti composites recorded before and after sintering for both compositions: (a) Series I (1 vol.% Ti) and (b) Series II (10 vol.% Ti)

in addition to the dominant α-Al_2O_3 phase, new reflections corresponding to Al_2TiO_5 (JCPDS 29-0053) and a small amount of TiO_2 (rutile, JCPDS 21-1276) were identified. Unlike in Series I, no evidence of $Ti_{0.25}Al_{1.75}O_3$ formation was found. Instead, the higher Ti content favored the formation of Al_2TiO_5, a compound typically produced by reaction between Al_2O_3 and TiO_2 at elevated temperatures. The simultaneous detection of residual TiO_2 indicates incomplete reaction, suggesting that under the applied sintering conditions, not all titanium was incorporated into a stable ternary phase. The absence of metallic Ti peaks after sintering confirms that titanium underwent complete

oxidation during thermal treatment, although its transformation pathway depended strongly on concentration. The observed differences can be rationalized by considering the role of titanium content in the reaction kinetics and phase equilibria. At low Ti addition (Series I), the fine dispersion and limited quantity of metallic titanium allowed complete interfacial reaction with Al_2O_3, yielding a single ternary phase ($Ti_{0.25}Al_{1.75}O_3$). In contrast, at higher Ti content (Series II), the reaction was less uniform, favoring the formation of Al_2TiO_5, accompanied by unreacted TiO_2. This difference is further consistent with the microstructural observations, where higher Ti content

led to agglomeration, poor dispersion, and increased porosity, all of which could limit diffusion and hinder complete phase transformation.

These results demonstrate a strong dependence of the final phase composition on the metallic phase content. While a low Ti fraction promotes the formation of a single, well-integrated reaction phase, higher Ti loadings give rise to multiphase products, including Al_2TiO_5 and residual oxides. Because Al_2TiO_5 exhibits anisotropic thermal expansion and limited thermal stability, its presence may impair the mechanical performance and thermal shock resistance of the composites. Consequently, controlling the Ti fraction and dispersion is crucial for tailoring the phase constitution and optimizing the functional properties of the Al_2O_3-Ti composites.

The particle size distribution of the metallic phase ($Ti_{0.25}Al_{1.75}O_3$ in Series I or Al_2TiO_5 in Series II forming particles) was analyzed for both composite series, differing in the volume fraction of metallic phase. The results are presented in Figure 6, where histogram (a) corresponds to Series I containing 1 vol% of the metallic phase, and histogram

(b) corresponds to Series II with 10 vol% metallic content. The parameter d_2 represents the equivalent circle diameter of the metallic particles.

In both series, the particle size distributions exhibit a distinctly right-skewed profile, characterized by a high frequency of small particles and a tail extending toward larger sizes. In Series I (Figure 6a), the mean particle size was 3.33 µm, with a standard deviation of ± 4.02 µm. The most frequent particle size range lies between 1.0 and 3.0 µm, with a pronounced peak around 1.4 µm. The presence of larger particles (>10 µm) was minimal, though a small fraction of particles exceeding 15 µm was also detected, likely corresponding to occasional large particles.

In contrast, Series II (Figure 6 b), which contains 10 vol% of the metallic phase, exhibited a slightly lower mean particle size of 3.27 µm and a slightly broader standard deviation of ± 4.08 µm. Although the most frequent particle size remained centered around 1.4 µm, the overall distribution was broader and displayed a greater frequency of particles within the 5–10 µm and >15 µm ranges. The broader particle size distribution observed in
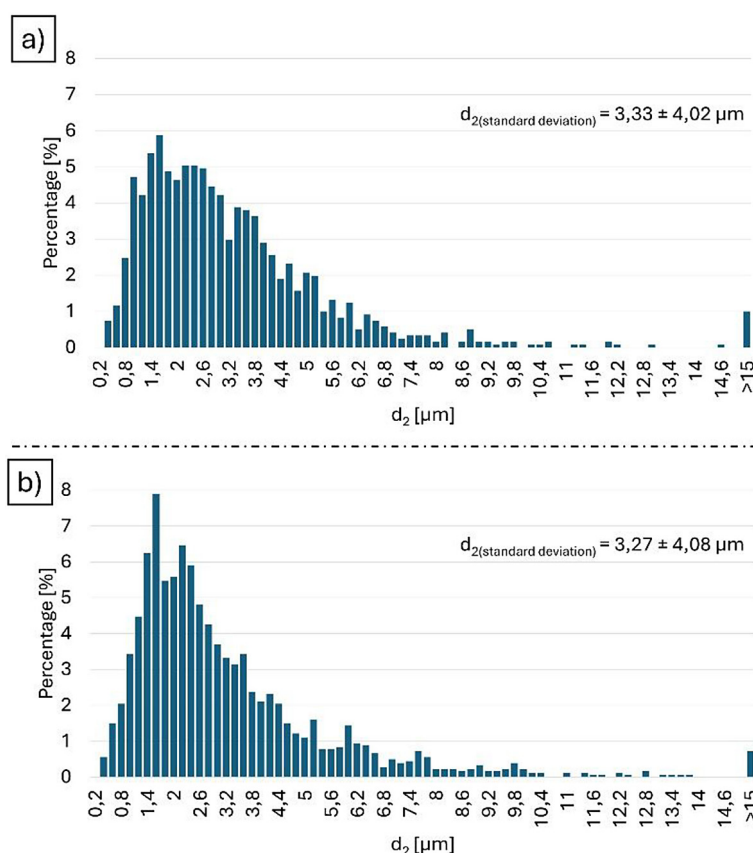
Figure 6. Particle size distribution histograms of metallic phase particles ($Ti_{0.25}Al_{1.75}O_3$ in Series I or Al_2TiO_5 in Series II forming) in the composite matrix: (a) Series I containing 1 vol.% metallic phase, and (b) Series II containing 10 vol.% metallic phase. The distributions are based on equivalent circle diameter (d_2) measurements

Series II suggests that increasing the metallic phase content promotes a greater tendency for particle aggregation or clustering, likely due to enhanced interparticle interactions at higher concentrations.

These observations indicate that the primary size distribution of the metallic particles remains relatively consistent regardless of the volume fraction, which confirms that the processing parameters were uniform across both series. However, the increase in volume fraction from 1% to 10% results in a clear broadening of the particle size distribution, with a higher proportion of larger particles in Series II. This broadening may stem from the increased probability of local clustering or inadequate dispersion of metallic particles in the matrix during slurry preparation or solidification. The small but notable population of particles exceeding 15 µm in Series II further supports this interpretation.

From a microstructural perspective, this broader particle size distribution could have several implications for the composite properties. Larger metallic inclusions or agglomerates may act as stress concentrators or microstructural heterogeneities, potentially influencing the mechanical response of the material. Depending on the interfacial bonding and the distribution of the metallic phase, such features might enhance or impair mechanical performance, including strength and fracture toughness. Moreover, the spatial uniformity of metallic particles is also critical in achieving desirable thermal or electrical properties, particularly in the composites where the metallic phase is intended to serve as a conductive or reinforcing network.

In conclusion, while the overall particle size characteristics are similar between the two series, the increased content of the metallic phase in Series II contributes to a broader and more heterogeneous particle distribution. These differences should be taken into consideration when optimizing processing parameters to achieve uniform dispersion and tailored composite properties.

CONCLUSIONS

The present study demonstrated a systematic investigation of the Al_2O_3-Ti composites fabricated by slip casting with two different metallic phase contents (1 vol.% and 10 vol.% Ti). A multi-technique approach, including rheological measurements, physical property analysis, SEM/EDS characterization, XRD phase analysis, and particle size distribution studies, enabled a comprehensive evaluation of how the Ti content influences slurry behavior, densification, phase constitution, and microstructural evolution.

The results show that the viscosity of suspensions strongly depends on the Ti fraction. The composite containing 1 vol.% Ti exhibited significantly higher viscosity due to the higher proportion of ultrafine alumina. In contrast, the 10 vol.% Ti suspension demonstrated lower viscosity, facilitating shaping but promoting phase segregation during casting. The results highlighted that early rheological behavior predetermines the final quality of the sintered composites.

The sintered composites revealed strikingly different densification behaviors. Series I (1 vol.% Ti) reached high relative density (>93%) with minimal porosity and uniform shrinkage, while Series II (10 vol.% Ti) suffered from poor densification (~77%), high open porosity, and anisotropic shrinkage. SEM analysis confirmed that low Ti content favors a dense and homogeneous microstructure with isolated metallic inclusions, while higher Ti content led to agglomeration, microcracking, and interfacial debonding. This degradation at higher Ti fractions stems from the poor packing of large Ti particles, mismatch in thermal expansion coefficients, and hindered diffusion during sintering.

Phase analysis by XRD revealed a clear dependence of reaction pathways on Ti fraction. At low Ti content, metallic Ti was completely consumed, forming a single ternary phase $(Ti_{0.25}Al_{1.75}O_3)$ with alumina. In contrast, at higher Ti content, oxidation resulted in the formation of Al_2TiO_5 and residual rutile TiO_2. Since Al_2TiO_5 is known for its poor thermal stability and anisotropic expansion, its presence may reduce the mechanical and thermal shock resistance of the composites. This observation provides valuable guidance for controlling the Ti additions in future designs of ceramic–metal composites.

The particle size distribution of metallic inclusions further supports these findings. Both series exhibited a skewed distribution dominated by small particles, but higher Ti content caused a broadening of the distribution and increased presence of larger agglomerates, acting as stress concentrators. This microstructural heterogeneity is consistent with the poorer densification and mechanical integrity observed in Series II.

Most previous studies on Al_2O_3-Ti composites have emphasized powder metallurgy, hot

pressing, or spark plasma sintering routes, often focusing on mechanical testing of fully dense composites. While slip casting has been employed for oxide-based systems, its application to Al_2O_3-Ti is scarcely reported, and few works systematically connect slurry rheology, densification, and phase evolution.

The main conclusions of this study can be summarized as follows:

- rheology-microstructure link – the viscosity of the casting slip, controlled by the Ti content, directly determines particle packing, densification, and porosity in the sintered composites;
- Ti-dependent phase evolution – at 1 vol.% Ti, the metallic phase is fully consumed to form the stable $Ti_{0.25}Al_{1.75}O_3$, while at 10 vol.% Ti, unstable Al_2TiO_5 and residual TiO_2 are produced;
- impact of excessive Ti – higher Ti content leads to agglomeration, poor dispersion, and high porosity, which are expected to degrade mechanical performance;
- practical significance – slip casting with optimized Ti content (1 vol.%) enables fabrication of dense, defect-free Al_2O_3-Ti composites, offering potential for structural, aerospace, and biomedical applications.

Compared to earlier research that often treated Ti simply as a toughening additive in Al_2O_3, this study revealed that its concentration must be carefully optimized to avoid detrimental phase transformations (formation of Al_2TiO_5) and processing-induced heterogeneities. Thus, the work provides both methodological novelty—through its comprehensive multi-scale analysis—and practical guidelines for tailoring the Al_2O_3-Ti composites processed by slip casting.

Acknowledgment

REFERENCES

1. Jia Y., Ajayi TD., Wahls BH., Ramakrishnan KR., Ekkad S., Xu C. Multifunctional ceramic composite system for simultaneous thermal protection and electromagnetic interference shielding for carbon fiber-reinforced polymer composites. ACS Applied Materials & Interfaces 2020; 12: 58005–58017. https://doi.org/10.1021/acsami.0c17361

2. Lakhdar Y., Tuck C., Binner J., Terry A., Goodridge R. Additive manufacturing of advanced ceramic materials. Progress in Materials Science 2021; 116: 100736. https://doi.org/10.1016/j.pmatsci.2020.100736

3. Ali MS., Ariff AHM., Hashmi MSJ., Brabazon D. Metal particles as additives in ceramic composite materials: A review of mechanical properties and their origin. In: Brabazon D., editor. Encyclopedia of Materials: Composites. Elsevier 2018; 145–157. https://doi.org/10.1016/B978-0-12-803581-8.10538-7

4. Mitoseriu L., Lukacs VA., Padurariu L., Ciomaga CE., Gheorghiu F., Horchidan N., Giuranno D. Emergent electrical properties in metal-ceramic composites: A critical revue. Ceramics International 2025. https://doi.org/10.1016/j.ceramint.2025.07.137

5. Jose S.A., John M., Menezes P.L. Cermet systems: Synthesis, properties, and applications. Ceramics 2022; 5(2): 210–236. https://doi.org/10.3390/ceramics5020018

6. Binner J., Porter M., Baker B., et al. Selection, processing, properties and applications of ultra-high temperature ceramic matrix composites, UHTC-MCs – a review. International Materials Reviews 2020; 65(7): 389–444. https://doi.org/10.1080/09506608.2019.1652006

7. Mehta A., Vasudev H. Advancements in ceramic-coated metals: Enhancing thermal spray coatings for improved performance in aerospace applications using surface treatments. Results in Surfaces and Interfaces 2025; 18: 100387. https://doi.org/10.1016/j.rsurfi.2024.100387

8. Grossin D., Montón A., Navarrete-Segado P., Özmen E., Urruth G., Maury F., Maury D., Frances C., Tourbin M., Lenormand P., Bertrand G. A review of additive manufacturing of ceramics by powder bed selective laser processing (sintering / melting): Calcium phosphate, silicon carbide, zirconia, alumina, and their composites. Open Ceramics 2021; 5: 100073. https://doi.org/10.1016/j.oceram.2021.100073

9. Wicaksono RA., Ardeshiri Lordejani A., Bagherifard S. Current trends and future perspective for cold spray metal-ceramic composites. Advanced Engineering Materials 2025; 27: 2401657. https://doi.org/10.1002/adem.202401657

10. Biluš Abaffy N., McCulloch DG., Partridge JG., Evans PJ., Triani G. Engineering titanium and aluminum oxide composites using atomic layer deposition. Journal of Applied Physics 2011; 110(12): 123514. https://doi.org/10.1063/1.3667134

11. Klimov AS., Bakeev IY., Oks EM., Zenin AA. Electron-beam sintering of an Al_2O_3/Ti composite using a forevacuum plasma-cathode electron source. Ceramics International 2020; 46(14): 22276–22281.

https://doi.org/10.1016/j.ceramint.2020.05.306

12. Sousa L., Antunes RDM., Fernandes JCS., Alves AC., Toptan F. Influence of Al_2O_3 reinforcements and Ti-Al intermetallics on corrosion and tribo-corrosion behavior of titanium. Surface and Coatings Technology 2023; 470: 129835. https://doi.org/10.1016/j.surfcoat.2023.129835

13. Bogdanov AI., Kulevich VP., Shmorgun VG., Gurevich LM. Structure and properties of Ti-Al intermetallic coatings reinforced with an aluminum oxide filler. Metals 2024; 14(12): 1336. https://doi.org/10.3390/met14121336

14. Azarniya A., Abdollah-zadeh A., Taheri-Nassaj E. Enhanced wear and corrosion resistance of Al–Al_2O_3 surface composites via hybridization by Alx-Tiy nanophase intermetallics. Journal of Materials Research and Technology 2025; 37: 5308–5331. https://doi.org/10.1016/j.jmrt.2025.07.156

15. Abyzov AM. Aluminum oxide and alumina ceramics (review). Part 1. Properties of Al_2O_3 and commercial production of dispersed Al_2O_3. Refractories and Industrial Ceramics 2019; 60: 24–32. https://doi.org/10.1007/s11148-019-00304-2

16. Parikh PB. Alumina ceramics: Engineering applications and domestic market potential. Transactions of the Indian Ceramic Society 1995; 54(5): 179–184. https://doi.org/10.1080/0371750X.1995.10804716

17. Wang J., Yang Z., Zhou B., Zhang H., Cui L., Niu Y., Rui X. In-depth study on tensile properties and finite element analysis of TiC in-situ formed Ti matrix composites with NbC and ZrC additions. Journal of Materials Research and Technology 2025; 35: 2188–2201. https://doi.org/10.1016/j.jmrt.2025.01.181

18. Gao K., Zhang Y., Yi J., Dong F., Chen P. Overview of surface modification techniques for titanium alloys in modern material science: A comprehensive analysis. Coatings 2024; 14(1): 148. https://doi.org/10.3390/coatings14010148

19. Yang J., Song Y., Dong K., Han EH. Research progress on the corrosion behavior of titanium alloys. Corrosion Reviews 2023; 41(1): 5–20. https://doi.org/10.1515/corrrev-2022-0031

20. Ammisetti DK., Kruthiventi SSH., Vinjavarapu S., et al. A review on reinforcements, fabrication methods, and mechanical and wear properties of titanium metal matrix composites. Journal of Engineering and Applied Science 2024; 71: 60. https://doi.org/10.1186/s44147-024-00392-z

21. Liang L., Wei B., Zhang M., Fang W., Chen L., Wang Y. Novel TiC-based ceramic with enhanced mechanical properties by reaction hot-pressing at low temperature. Journal of Materials Research and Technology 2023; 24: 2129–2143. https://doi.org/10.1016/j.jmrt.2023.03.111

22. Tshephe TS., Akinwamide SO., Olevsky E., Olubambi PA. Additive manufacturing of titanium-based alloys – A review of methods, properties, challenges, and prospects. Heliyon 2022; 8(3): e09041. https://doi.org/10.1016/j.heliyon.2022.e09041

23. Meir S., Kalabukhov S., Frage N., Hayun S. Mechanical properties of Al_2O_3/Ti composites fabricated by spark plasma sintering. Ceramics International 2015; 41(3, Part B): 4637–4643. https://doi.org/10.1016/j.ceramint.2014.12.008

24. Rocha-Rangel E., Refugio-García E., Miranda-Hernández JG., Térres-Rojas E., de la Torre SD. Preparation and their mechanical properties of Al_2O_3/Ti composite materials. In: Mathur S., Shen H., Singh M., editors. Nanostructured Materials and Systems. 2010. https://doi.org/10.1002/9780470909812.ch12

25. Bahraminasab M., Arab S., Ghaffari S. Osteoblastic cell response to Al_2O_3-Ti composites as bone implant materials. BioImpacts 2022; 12(3): 247–259. https://doi.org/10.34172/bi.2021.2330

26. Manes A., Giglio M. Microstructural numerical modeling of Al_2O_3/Ti composite. Procedia Structural Integrity 2018; 8: 24–32. https://doi.org/10.1016/j.prostr.2017.12.004

27. Hutsaylyuk V., Student M., Posuvailo V., Student O., Sirak Y., Hvozdets'kyi V., Maruschak P., Veselivska H. The properties of oxide-ceramic layers with Cu and Ni inclusions synthesizing by PEO method on top of the gas-spraying coatings on aluminium alloys. Vacuum 2020; 179: 109514. https://doi.org/10.1016/j.vacuum.2020.109514

28. Hutsaylyuk V., Student M., Posuvailo V., Student O., Hvozdets'kyi V., Maruschak P., Zakiev V. The role of hydrogen in the formation of oxide-ceramic layers on aluminum alloys during their plasma-electrolytic oxidation. Journal of Materials Research and Technology 2021; 14: 1682–1696. https://doi.org/10.1016/j.jmrt.2021.07.082

29. Laszkiewicz-Łukasik J., Putyra P., Klimczyk P., Podsiadło M., Bednarczyk K. Spark plasma sintering/field assisted sintering technique as a universal method for the synthesis, densification and bonding processes for metal, ceramic and composite materials. Journal of Applied Materials Engineering 2020; 60; 2–3. 10.35995/jame60020005

30. Ujah CO., Von Kallon DV., Aigbodion VS. High entropy alloys prepared by spark plasma sintering: Mechanical and thermal properties. Materials Today Sustainability 2024; 25: 100639. https://doi.org/10.1016/j.mtsust.2023.100639

31. Cavaliere P., Sadeghi B., Shabani A. Spark Plasma Sintering: Process Fundamentals. Spark Plasma Sintering of Materials: Advances in Processing and Applications. Springer International Publishing; 2019; 3–20.

32. Le Ferrand H. Magnetic slip casting for dense and textured ceramics: A review of current achievements

and issues. Journal of the European Ceramic Society 2021; 41(1): 24–37. https://doi.org/10.1016/j.jeurceramsoc.2020.08.030

33. Meshalkin VP., Belyakov AV. Methods used for the compaction and molding of ceramic matrix composites reinforced with carbon nanotubes. Processes 2020; 8(8): 1004. https://doi.org/10.3390/pr8081004

34. Shahrestani S., Ismail MC., Kakooei S., Beheshti M. Effect of additives on slip casting rheology, microstructure and mechanical properties of Si3N4/SiC composites. Ceramics International 2020; 46(5): 6182–6190. https://doi.org/10.1016/j.ceramint.2019.11.085

35. Wiecinski P., Wieclaw-Midor A. Slip casting of highly concentrated ZnO suspensions: Rheological studies, two-step sintering and resistivity measurements. Ceramics International 2020; 46(12): 19896–19903. https://doi.org/10.1016/j.ceramint.2020.05.051

36. Łada P., et al. Fabrication of ZrO_2-Ti composites by slip casting method. Archives of Metallurgy and Materials 2016; 61: 1095–1100.

37. Wachowski M., Zygmuntowicz J., Kosturek R., Piotrkiewicz P., Żurowski R., Więcław-Midor A., Śnieżek L. Study on manufacturing via slip casting and properties of alumina-titanium composite enhanced by thialite phase. Materials 2023; 16(1): 79. https://doi.org/10.3390/ma16010079

38. Vukšić M., Žmak I., Ćurković L., Ćorić D. Effect of additives on stability of alumina—waste alumina suspension for slip casting: Optimization using Box-Behnken design. Materials 2019; 12(11): 1738. https://doi.org/10.3390/ma12111738

39. Michalski J., Wejrzanowski T., Pielaszek R., Konopka K., Łojkowski W., Kurzydłowski KJ. Application of image analysis for characterization of powders. Materials Science Poland 2005; 23: 79–86.

40. Wejrzanowski T., Kurzydłowski K.J. Stereology of grains in nano-crystals. Solid State Phenomena 2003; 94: 221–228. https://doi.org/10.4028/www.scientific.net/SSP.94.221

41. Wejrzanowski T., Spychalski W., Rożniatowski K., Kurzydłowski K. Image-based analysis of complex microstructures of engineering materials. International Journal of Applied Mathematics and Computer Science 2008; 18: 33–39. https://doi.org/10.2478/v10006-008-0003-1

42. Kurzydłowski KJ., Ralph B. The Quantitative Description of the Microstructure of Materials. CRC Press 1995.

43. Falkowski P., Żurowski R. Shaping of alumina microbeads by drop-casting of the photopolymerizable suspension into silicone oil and UV curing. Journal of the European Ceramic Society 2022. https://doi.org/10.1016/j.jeurceramsoc.2022.03.014

44. Alcázar C., Moreno R. Manufacture of titania foams by replica method and infiltration with anatase nanoparticles. European Journal of Materials 2023; 3: 2225542. https://doi.org/10.1080/26889277.2023.2225542

45. Wiecinska P., Zurawska A., Falkowski P., Jeong D-Y., Szafran M. Sweet ceramics: How saccharide-based compounds have changed colloidal processing of ceramic materials. Journal of the Korean Ceramic Society 2020; 57: 231–245. https://doi.org/10.1007/s43207-020-00036-x

46. Hossain SS., Gao B., Park S., Bae C-J. Incorporating nanoparticles in alumina ink for improved solid-loading and sinterability of extrusion-based 3D printing. ACS Applied Nano Materials 2022; 5: 17828–17838. https://doi.org/10.1021/acsanm.2c03792

47. Żurowski R., Zygmuntowicz J., Tomaszewska J., Ulkowska U., Piotrkiewicz P., Wachowski M., Szachogłuchowicz I., Kukielski M. Sustainable ZTA composites produced by an advanced centrifugal slip casting method. Ceramics International 2022; 48: 11678–11695. https://doi.org/10.1016/j.ceramint.2022.01.026